REVISION 1

Shock-induced mobilization of metal and sulfide in planetesimals: Evidence from the Buck Mountains 005 (L6 S4) dike-bearing chondrite

**Alex Ruzicka[1, 2, *], Ryan Brown[1], Jon Friedrich[3, 4],
Melinda Hutson[1, 2], Richard Hugo[2] and Mark Rivers[5]**

[1] Cascadia Meteorite Laboratory, Portland State University, 1721 SW Broadway, Portland, Oregon 97207, U.S.A.

[2] Department of Geology, Portland State University, 17 Cramer Hall, 1721 SW Broadway, Portland, Oregon 97207, U.S.A.

[3] Department of Chemistry, Fordham University, Bronx, New York 10458, U.S.A.

[4] Department of Earth and Planetary Sciences, American Museum of Natural History, New York, New York 10024, U.S.A.

[5] Consortium for Advanced Radiation Sources, University of Chicago, Argonne, Illinois 60439, U.S.A.

* email: ruzickaa@pdx.edu

Revised May 20, 2015

ABSTRACT

The conditions under which metal cores formed in silicate-metal planetary bodies in the early solar system are poorly known. We studied the Buck Mountains 005 (L6) chondrite with serial sectioning, X-ray computed microtomography, and optical and electron microscopy to better understand how metal and troilite were redistributed as a result of a moderately strong (shock stage S4) shock event, as an example of how collisional processes could have contributed to differentiation. The chondrite was recovered on Earth in multiple small pieces, some of which have a prominent, 1.5-3-mm-wide holocrystalline shock melt dike that forms a jointed, sheet-like structure, as well as an associated shock vein network. The data suggest that metal and troilite within the dike were melted, sheared, and transported as small parcels of melt, with metal moving out of the dike and along branching veins to become deposited as coarser nodules and veins within largely unmelted host. Troilite also mobilized but partly separated from metal to become embedded as finer-grained particles, vein networks, and emulsions intimately intergrown with silicates. Rock textures and metal compositions imply that shock melts cooled rapidly against relatively cool parent body materials, but that low-temperature annealing occurred by deep burial within the parent body. Our results demonstrate the ability of shock processes to create larger metal accumulations in substantially unmelted meteorite parent bodies, and have implications for the formation of iron meteorites and for core formation within colliding planetesimals.

Keywords: LUNAR AND PLANETARY STUDIES: shock metamorphism, METEORITE: L6 chondrite, PETROGRAPHY: chondrite, olivine, kamacite, taenite, troilite, ELECTRON MICROSCOPY: olivine, FeNi metal, troilite

INTRODUCTION

The segregation of metal and ultimate formation of metal cores during differentiation was one of the most fundamental processes to affect silicate-metal planetary bodies in the early solar

1

system, but the conditions under which such differentiation occurred is poorly understood. Gravity-induced metal separation is likely at high melting degree, such as in magma oceans, but is more problematic by porous flow in hydrostatic conditions when silicate is mostly solid, owing to the high interfacial energy between iron-sulfide metallic melt and silicate solid (high dihedral angle of metallic melt), which prevents metallic melts from interconnecting (e.g., Minarek et al., 1996; Shannon and Agee, 1996; Gaetani and Grove, 1999). Even at moderate degrees of melting when silicate is partly molten, metallic melt might not interconnect and efficiently separate (Rushmer et al., 2005; Rushmer and Petford, 2011). However, experiments and numerical models suggest that interconnection of metallic melts is greatly facilitated by shear deformation (Bruhn et al., 2000; Groebner and Kohlstedt, 2006; Kohlstedt and Holzman, 2009; Rushmer et al., 2000, 2005; Rushmer and Petford, 2011). Similarly, observations of chondritic meteorites suggest that shock processes could have played an important role in mobilizing and segregating metal from silicate and sulfide (e.g., Rubin, 2002; Tomkins et al., 2013a), producing both metal-veined chondrites such as Portales Valley (Kring et al., 1999; Rubin et al., 2001; Ruzicka et al., 2005) and Kernouvé (Friedrich et al., 2013), as well as coarser nodules of metal (Widom et al., 1986; Fujita et al., 1999; Rubin, 1999). This process could have contributed to core formation in planetesimals (Tomkins et al., 2013a, b). Studies of chondrites are revealing as many were shock-deformed under conditions of both low gravity and low melting degree, providing direct evidence for the efficacy of shock alone to segregate metal.

In this work, we studied the Buck Mountains 005 (L6) chondrite, which is notable for containing a prominent, metal-depleted shock melt dike (Brown et al., 2013a, b; Hutson et al., 2013a, b) and also unusually coarse metal in the adjacent host. This distribution of metal suggests the possibility of metal segregation processes during dike formation. The meteorite was studied

with serial sectioning, X-ray computed microtomography, and optical and electron microscopy. Our results have implications for impact-induced segregation of metal in planetary bodies.

METHODS AND SAMPLES

The Buck Mountains 005 chondrite (hereafter BM005), also known as Yucca 014 (MBD, 2014), is classified as an L6 chondrite of shock stage S4 and weathering grade W2, with approximately half of the metal weathered (Ruzicka et al., 2014). BM005 was recovered as 36 pieces in a 1.3 x 1.3 m^2 area on the same day (Ruzicka et al., 2014). Some of the smaller pieces (~1-3 cm^3) contain a ~1.5-3-mm-wide dike, which appears in hand specimens as a dark banded feature, with a columnar surface expression normal to the dike (Fig. 1a). Two such pieces (designated CML0491-3 and CML0491-5) are the focus of this study. Polished thin sections 0491-3A and 0491-5-2 were prepared from the -3 and -5 specimens, respectively, and were studied with optical microscopy and electron microscopy. One end of the 0491-5 piece was additionally used for X-ray computed microtomography and serial sectioning, prior to thin section preparation of one of the thin slices.

Optical and scanning electron microscopy

Samples were studied at Portland State University using a Leica EZ binocular microscope, a Leica DM2500 petrographic microscope, and a Zeiss Sigma FE-VP scanning electron microscope (SEM). The binocular microscope was used to image thin slices and cut fragments produced during serial sectioning as well as thin sections, and the petrographic microscope and SEM were used to examine fine-scale features in polished thin sections. Optical microscopy was used to study shock features and to obtain digital images obtained in three different light modes (transmitted plane-polarized, transmitted cross-polarized, and reflected), with images assembled into mosaics using Adobe Photoshop software. To assess olivine deformation, the method of Jamsja and Ruzicka (2010) was used to assign shock stages (Stöffler et al., 1991) to individual olivine grains in the

3

0491-5-2 section, relying mainly on variations in extinction position of olivine as seen in cross-polarized transmitted light. Such variations are a manifestation of plastic deformation. With this method, both a conventional shock stage (the highest shock stage shown by at least 25% of the grains—Stöffler et al., 1991) and a weighted shock stage (the mean grain shock stage) was determined. Maskelynite, an amorphous form of feldspar produced by shock, was confirmed by isotropic character. SEM data included backscattered electron (BSE) images, and microchemical data obtained with X-ray energy dispersive spectroscopy (EDS) using a high-speed, large area (50 mm^2), silicon-drift detector. Quantitative chemical data were obtained in the form of points and line scans and as calibrated X-ray intensity map images using AZtec 2.2 software. AZtec was used to create false color EDS phase maps and montages by combining colorized X-ray intensity images for different elements. Reflected light and EDS montages were used for modal analysis, using Photoshop to create masks, and ImageJ 1.44 software with the Color Inspector 3D plug in (Wu Quant module) to analyze color values and proportions. Spatial resolutions of the mosaics used for modal studies were 4.1-4.3 µm/pixel. Errors (precisions) of modal determinations were equated to the standard deviation of mean phase proportions in three separate determinations of a given data set, using variations in Wu Quant parameters (numbers of colors) and phase color assignments, excluding apparent phase mixtures.

X-ray computed microtomography

Synchrotron X-ray computed microtomography (µCT) (Ebel and Rivers, 2007) was used to study the three-dimensional distribution of metal and other phases in the dike and surrounding rock. Data were obtained at the GSECARS beamline 13-BMD at the Advanced Photon Source with monochromatic 46.6 keV X-rays at resolutions of 7.7 and 9.3 µm/voxel (a voxel is a 3D volume element akin to a 2D pixel). Phases of differing X-ray attenuation corresponding to metal, sulfide, weathering product of metal and sulfide, silicate, and voids were imaged in three different data sets

4

and portrayed in tomogram slices and video stacked slices (movies) in three orthogonal directions for each data set. Sulfide and hydrated metal-sulfide weathering products ($Fe_xO_yOH_z$) have nearly identical X-ray attenuation coefficients and were treated as a single phase in μCT data sets, although subtle differences often allow their discrimination in tomography images. Particles were digitally isolated using BLOB3D software (Ketchum, 2005) on the basis of greyscale thresholding. These particles were used for quantitative analysis (particle sizes and volumes) and the construction of 3D visualization models.

RESULTS

Serial sectioning results

The small piece of BM005 studied by serial sectioning was a complete specimen, bounded on one side by fusion crust and on all other sides by a naturally fragmented surface; the dike runs through and across the middle of the specimen (Fig. 1a). On fragmented surfaces showing the dike, a columnar surface texture roughly perpendicular to the dike extends across the dike and partly into the surrounding host (Fig. 1a). Two dark surface patinas on raised surfaces, which are not fusion crust, occur on relatively flat sides of the specimen at an intermediate angle (~40-65°) to the dike (Fig. 1a).

Three parallel cuts made perpendicular to the dike and an additional cut made perpendicular to these cuts exposed eight interior surfaces. These cut surfaces show that the dike forms a nested sheet-like structure with an inner and outer portion, and that side veins are present which branch from the dike or run semi-parallel to it (Fig. 1b). The dike and veins appear dark grey in cut surfaces and are depleted in metal, but some veins connect to coarser metal that is present near the surface of the meteorite, away from the dike (Fig. 1b). Sectioning through one of the raised patinas exposed coarser metal below the patina (Fig. 1c). This suggests that the patinas are the weathered surface expression of metal-rich sheets. Regularly-spaced fractures roughly perpendicular to the dike extend

5

across the dike and partly into the surrounding host. These fractures explain the columnar surface texture observed in the pre-cut specimen, as their presence would allow the surface of the dike to fragment and break off in columns.

Optical and electron microscopy results for the dike

The overall structure of the dike is similar in both polished sections examined of two different specimens, and consists of a zoned inner-outer dike structure, with the inner dike containing mineral and lithic clasts ≤0.4 mm across and the outer dike being nearly clast-free (Fig. 2a). Both parts of the dike are composed chiefly of fine-grained silicates (≤10 μm across) of mafic character (olivine- and pyroxene-like compositions) that have an igneous texture. Larger grains of metal and troilite are depleted in the dike compared to the surrounding host (Fig. 2b), although considerable fine-grained troilite occurs in the inner dike and on its margins (Fig. 2c). The regularly-spaced cracks that occur mainly within and at a high angle (nearly perpendicular) to the dike cut across all features and are often partly filled with weathering product (Fig. 2b). The outermost edge of the dike near the host is typically marked by a thin band of magnesian silicates (olivine, low-Ca pyroxene), possibly a chill zone (Fig. 2d).

The inner dike is flanked by troilite-rich bands (Fig. 2b, 2c). In detail these bands are composed of an intergrowth of troilite and weathering product of metal (Ni-bearing hydroxide) that is interstitial to silicates (Fig. 2e). Some of the silicates in the troilite-rich band are euhedral or subhedral and similar to that elsewhere in the dike, whereas others appear to be mineral clasts (Fig. 2e). The texture of these bands suggests the former presence of silicate entrained in FeNiS metallic melt.

In the outer dike, metal and troilite are depleted and are present in the form of small (~5-40-μm-diameter) globules, which are locally concentrated in clusters adjacent to host (Fig. 2c, 2d, 2f). The globules consist mainly of an intergrowth of troilite and weathering product of metal, or more

6

rarely, of troilite and unaltered metal (Fig. 2f). In both, globules have a cellular texture of quasi-regularly-spaced metal (or metal weathering product) within troilite, reminiscent of rapidly-solidified metal-sulfide melt globules in shocked meteorites (Scott, 1982) but on a finer scale. These spacings potentially can be related to cooling rate (Scott, 1982). Metal cell spacings (metal center to metal center) measured in fourteen dike globules are 3.8 ± 1.1 µm (mean and standard deviation). Less commonly, globules consist of metal weathering product alone (Fig. 2f).

Veins of troilite + hydroxide or troilite + metal extend across both the inner and outer dike roughly perpendicular to it (Fig. 2c). These veins do not cross both the inner and outer dike at any given location but rather begin or end in the troilite-rich band at the edge of the inner dike. However, the veins in the outer dike sometimes extend into the host for a short distance (Fig. 2c). In one location in the inner dike, a troilite-rich vein cuts across clasts.

Interstitial to fine-grained silicates both in the inner and outer dike, a fine-grained Fe-rich symplectite phase is present (Fig. 2f). Chemical data suggest the symplectite is nearly Ni-free Fe-hydroxide or Fe-oxide, unlike the Ni-bearing metal and metal weathering product found elsewhere in the dike. It may have formed by weathering of Ni-free metal produced by FeO-reduction of silicates.

Optical and electron microscopy results for the vein network

Side veins that branch from the dike or run semi-parallel to it contain minerals and clasts that are finer-grained than the dike (Fig. 2d), giving them an opaque appearance in transmitted light (Fig. 2a, 3a). The side veins are heterogeneous in their sulfide textures over distances as short as ~50-100 microns. Some areas contain extremely fine-grained mixtures of dispersed troilite (<0.3 µm across) and silicate (region T in Fig. 3d). In other (more typical) areas, fine-grained silicate is dominant (region S in Fig. 3d). In places the veins have concentrations of troilite-rich globules, usually coarser closer to the dike (up to 15 µm in diameter, Fig. 2d) and finer farther away (~1-2

7

μm in diameter, region G in Fig. 3d). In still other areas, mainly on the edges of the side veins or of larger clasts, troilite forms coarser, vein-like emulsions (region E in Fig. 3d). In some areas of host adjacent to side veins and in clasts within the veins, the interstices of brecciated silicate are filled with microveins (~1-10 μm wide) of troilite, troilite + feldspar (or maskelynite), or feldspar (maskelynite) (Fig. 2d).

Coarse metal is locally present in the host meteorite and interconnects with the side veins (Fig. 3a, 3b, 3c). The coarse metal in the 0491-5-2 section (Fig. 2b, 3a) is composed of kamacite, zoned taenite (with Ni-rich margins adjacent to kamacite), and plessite, and is intergrown with a smaller proportion of troilite (Fig. 3b). Other than coarse size, this metal resembles smaller metal grains in the BM005 host in containing both kamacite and zoned taenite. Line scan data of the largest taenite grains (nodule and other grains) in BM005 indicate well-formed M-shaped Ni profiles in taenite, with central Ni contents of ~23-20 wt% corresponding to taenite grain radii of ~50-135 μm, respectively.

There are at least five connection points between shock veins and the coarse metal (Fig. 3b, 3c). At most connection points there is an abrupt transition between silicate-rich shock vein and coarse metal (Fig. 3c), but in one area (point 3, Fig. 3b) silicate vein material extends into and ultimately merges with the coarse metal.

Shock petrography of silicates

Optical microscopy was used for a detailed study of shock effects in BM005 silicates. Feldspar is crystalline throughout most of the host, but is found as maskelynite adjacent to the dike and side veins. Such maskelynite is characteristic of shock stage S5 (Stöffler et al., 1991). For olivine, the data indicate for the host (based on N=80 grains) a conventional shock stage of S4 (~53% of the grains are S4), and a weighted shock stage of 3.48 (grains deformed to S3 and S4 levels are most common). For clasts in the inner dike (N=13), the conventional shock stage is S5

8

(~46% of the grains are S5), and the weighted shock stage is 4.54 (grains deformed to S4 and S5

levels are most common). The data show that the rock overall was affected by a moderately strong

("S4") shock, and that silicates within and near the dike and side veins were more strongly

deformed (to roughly "S5" levels). The spread of grain shock stages is not especially large,

providing no evidence that BM005 is a breccia or that the rock was affected by more than one major

impact event. Similarly, the concentration of maskelynite around the dike and side veins shows that

maskelynite was created by the shock event that produced these features.

Micro-CT results

Microtomography reveals important features about the three-dimensional distribution of

dike materials and of metal and sulfide in BM005. Figure 4 shows tomogram slices at different

depths along a single direction in sample CML0491-5, with a perspective similar to that in Fig. 1b

and 2b. The overall dike forms a sheet of generally consistent thickness and is confirmed to be

metal-depleted, except notably for patches of metal-bearing globules visible in the outer dike (Fig.

4c). In contrast, the inner dike, which is visible by outlines of likely sulfide-rich material, varies

greatly in thickness. In places the inner dike has thicker and thinner portions but forms a continuous

structure (Fig. 4a), as observed in thin section (Fig. 2b). In other places the inner dike pinches out to

form lens-shaped features (Fig. 4b, 4c, 4d). These lens-shaped features resemble boudins, and in

places they have asymmetric outlines that appear similar to mineral "fish" in shear zones (Passchier

and Trouw, 2005). Based on such asymmetries, dextral shear across either side of the inner dike can

be inferred for the perspective in Fig. 4 (Fig. 4b, 4d). Cracks perpendicular to the dike are

confirmed to be mostly confined to the dike, and partly filled with likely weathering product,

mainly in the inner dike (Fig. 4a).

The micro-CT results also demonstrate the presence of multiple coarse metal grains

("nodules") in the host. Some nodules, including the largest, occur near the dike (Fig. 4d), whereas

9

others occur farther from the dike (Fig. 4a, 4d). Nodule metal is sometimes but not always

surrounded by material of medium X-ray attenuation (light grey in Fig. 4) that could be sulfide, or

weathering product of metal or sulfide. Based on comparison with microscopy data, weathering

product can sometimes be identified in µCT images, either by the presence of internal voids, by

morphology as sheaths surrounding coarse metal, or by a slightly darker appearance than sulfide.

Using these criteria it appears that the light grey material in Fig. 4 associated with metal nodules

composed of both weathering product and a larger proportion of sulfide. This would indicate that

some coarse sulfide is also present in nodules in addition to coarse metal, more extensive when it

occurs than that observed in thin sections (Fig. 3b). A characteristic feature of such nodules in

BM005 is the presence of silicates that are confirmed to be completely embedded within both metal

and sulfide (seen in sulfide in Fig. 4c), as also implied in thin section (seen in metal in Fig. 3a and

3b).

Figure 5 shows models of the 3D distribution of metal and sulfide / weathering product in

the µCT-imaged volume of BM005. The 3D model clearly shows the depletion of metal in the dike

and the presence of metal nodules in the host (Fig. 5a). The eight largest metal particles (identified

in Fig. 5a) have volumes that range from ~0.86 mm^3 (#1) and ~0.45 mm^3 (#2) to ~0.01 mm^3 (#8).

These comprise ~75 vol% of the total metal in the µCT-imaged volume. The two largest particles,

here termed Nodule 1 and 2, alone comprise ~59 vol% of the total metal, highlighting the tendency

for metal to be present as nodules. Close study of µCT images indicates that Nodule 1 (1.70/1.25

mm in long/short axis) does not abut directly against the dike, but rather is located a short distance

away on the edge of a branching vein that forms a short arc on the edge of the dike. Similar

branching (arc-like) veins can be seen on the left side of the dike in the BSE mosaic of Fig. 2b and

in the optical image of Fig. 2a. Nodule 2 (1.45/0.68 mm in long/short axis) is located in the same

general location of the 0491-5 sample as the coarse metal observed in thin section (Fig. 2b, 3a, 3b)

10

and in cut faces (Fig. 1b). Nodule 2 as imaged with µCT could be an extension of the coarse metal

seen in thin section and saw cuts.

In contrast to metal, sulfide / weathering product is present throughout BM005 as smaller,

more numerous grains (Fig. 5b). The outer dike is depleted in sulfide / weathering product, except

notably for sheet-like structures that cross the outer dike roughly normal to the dike (Fig. 5b). Based

on analogy with features observed in thin section, these structures could be composed of both

weathering product and troilite-rich veins. The inner dike has more sulfide and weathering product

than the outer dike, including sheet-like structures that parallel the dike (Fig. 5b). Probably the latter

mainly correspond to troilite-rich bands.

Modal composition results

Modal data for metal, sulfide, and other phases in BM005 were obtained from analysis of

maps generated from reflected light (RL), chemical (EDS), and µCT imagery and are given in Table

1. Two issues are highlighted here: the total amount of metal and troilite in BM005, and the amount

of metal and troilite in the dike compared to the host. In both cases, the situation is complicated by

the presence of weathering product, which probably consists mainly of weathering product of metal

(~50% of metal weathered in BM005), and a smaller portion of weathering product of troilite

(certainly <50% of troilite weathered) and silicate.

With regard to the total amount of metal and troilite, RL modes for the 0491-3A and 0491-5-

2 sections show ~1 area% of troilite in both, and ~2 area% metal in 0491-5-2 (which contains

coarse metal), and ~0.9 area% metal in 0491-3A (which lacks coarse metal and is probably more

representative for metal) (Table 1). EDS modes for 0491-5-2 give a generally consistent value for

troilite (~1.5 area%) and metal (~2.5 area%), although much less weathering product was identified

for this section based on RL (~4.3 area% weathering + oxide minerals) than based on EDS (~7

11

area%) (Table 1). μCT data for the 0491-5 piece, which are probably most representative for

BM005 overall, suggest ~4.7 vol% troilite + weathering product and ~1 vol% metal.

Assuming that areas in representative sections can be equated to volumes in three

dimensions, the different data types can be reconciled to suggest ~1.5 vol% troilite and ~1 vol%

metal in BM005 overall. Assuming < 50% weathering for troilite and ~50% of metal weathered,

this suggests pre-weathering values of <3 vol% troilite and ~2 vol% metal in BM005 altogether.

With regard to metal and troilite in the dike compared to that in the host, EDS mapping data

for 0491-5-2 indicate a difference between metal and troilite. The dike is severely depleted in metal

and contains only trace amounts, compared to the host (4.0 ± 0.1 area%). In contrast, troilite is

enriched in the dike overall (2.1 ± 0.3 area%) compared to the host (1.6 ± 0.1 area%), reflecting

high concentrations in the inner dike (3.3 ± 0.2 area%) (Table 1). The high troilite value for the

inner dike is partly due to the presence of the flanking troilite-rich bands, which were counted as

part of the inner dike. A large amount of weathering product is present in the inner dike especially,

partly owing to the weathering products associated with the perpendicular cracks. Much of this

weathering product could have been transported from elsewhere and deposited within these cracks.

Besides differences in metal and troilite contents between the dike and host, the EDS

mapping data also indicate differences in the proportions of other phases. Feldspar, chromite, and

Ca-rich pyroxene (diopside) are all significantly depleted in the dike compared to the host, and

phosphate is absent in the dike (Table 1). The latter mineral probably grows during metamorphism

(Huss et al., 2005), so its absence in the dike can be explained by dike formation occurring after

thermal metamorphism. The other phases apparently were destroyed within the dike in favor of the

formation of mafic phases (olivine, low-Ca-pyroxene, and various Ca-poor pyroxene-like phases),

which are enriched in the dike. Although the mineralogy of the dike is enriched in high-melting-

temperature phases (mafic minerals), textural observations show clearly that the dike was

12

substantially molten and is not a restite. Instead, low-melting-temperature components (Ca-pyroxene, feldspar) were apparently moved out of the dike, possibly in response to high temperatures and pressures there.

DISCUSSION

Shock-induced melting and deformation

We suggest that the most important processes involved in forming the dike and side veins were simultaneous shock-induced melting and deformation. One major shock event, generally corresponding to shock stage S4 overall in the BM005 protolith, but locally involving more intense deformation and heating, evidently was responsible for producing the dike and side veins. The small proportion of clasts in the outer dike and the larger proportion in the inner dike suggest that the outer dike was almost fully molten and the inner dike was partly molten. Additional evidence for greater melting in the outer dike is provided by the prevalence of metal-sulfide globules there, whose spheroidal form can be explained as immiscible metallic melts within silicate melt. Metal-sulfide globules are commonly observed within experimentally-produced shock and other quenched melts of chondrites (Schmitt, 2000; Hörz et al., 2005; Rushmer et al., 2005) and naturally-produced shock melts of chondrules (e.g., Scott, 1982; Stöffler et al., 1991; Schepker, 2014). Largely molten dike material, including silicate and metallic melts, appears to have fed into the side veins, based on the gradation of textures between dike and branching side veins, and textures suggestive of apparent bulging into the latter.

Shear was probably important in producing the dike and side veins. Given that much of the dike and side veins were shock melted but that the chondrite host was largely unmelted, frictional melting (van der Bogert et al., 2003; Spray 2010) was probably responsible for enhancing melting along shear zones. Consistent with shear, μCT data suggest differential lateral movement across the inner dike, with the inner dike moving as a more competent unit within the outer dike and forming

13

boudin-like features. The textures of the troilite-rich bands on the edge of inner dike suggest that they were substantially molten, which could have allowed a mechanical decoupling between the inner and outer dike, and an accommodation of differential shear. Evidence for shear and boudin-like features bounded by metallic or sulfide-rich edges also have been found in the shock veins of other chondrites (Tomkins et al., 2013a), although the dike in BM005 is fairly unique so far as we know in showing such a distinct inner-outer zonal structure. Shear appears to have been concentrated along the margins of shock melt veins in some chondrites (Tomkins et al., 2013a), and by analogy we suggest that shear stress was maximized along the outer edge of the dike adjacent to the host chondrite.

Following melting and upon cooling, it appears joints developed in the dike and immediate surroundings. These joints formed the prominent cracks that are nearly perpendicular to the dike, and which became filled in many cases with weathering product.

Transport and accumulation of metal and sulfide

We suggest that metal and sulfide melts were transported and accumulated in different ways during shock. In BM005, metal is strongly depleted in the dike (Table 1, Fig. 5) and concentrated in coarser grains in the host, implying the net transport of metal from the dike to nodules in the host. Such transport almost certainly occurred through the side veins that connect the dike and nodules. Troilite was also redistributed, but in contrast to metal, it partly concentrated in the inner dike and in side veins, with a smaller proportion accumulating into coarser grains.

Evidence suggests that metal and troilite were transported initially in the form of immiscible melt globules, which were then progressively sheared into small parcels of metal and sulfide melt during a single episode of shock melting and deformation. The concentration of metal-troilite globules at the outer edge of the dike implies that melt globules were transported outwards. This can be accomplished by differential shearing, in which melt moves towards zones of high shear stress

14

(Kohlstedt and Holzman, 2009; Tomkins et al., 2013a). As melt globules moved outwards into zones of higher shear stress, they would have been disrupted, creating smaller globules. This explains the tendency for globules to become smaller towards the edge of the dike and to be present in pockets, both of which can be explained by the disruption of larger globules. Some of the melt globules moved into the side veins, where continued shearing would have made the globules still smaller, as observed. Indeed, shear would be expected to increase in narrower side veins by the effect of increased drag along narrow passage walls. Immiscible melt drops would become increasingly finer, until ultimately small parcels of disconnected metal and sulfide melt were present, producing a finely dispersed mixture of silicate, metal, and sulfide melt. Such a fine mixture would permit melts to move through even narrow passages in shock veins. The postulated mixture was perhaps similar to a combination of ultrafine silicate and sulfide that is preserved in side veins, plus metal of similar size that was not preserved.

The creation of a mixture with disconnected metal and sulfide melt, together with differences in the physical properties of these melts, could have allowed metal and sulfide melt to separate and to become redistributed in different ways in the side veins. The evidence from BM005 suggests that metal melt accumulated into larger patches, which largely passed through and separated from the silicate-rich side veins. In contrast, some sulfide was preserved in side veins in intimate association with silicate, forming ultrafine mixtures of sulfide and silicate, troilite microvein networks, and troilite-rich emulsions. Metal melt has a lower viscosity than sulfide melt, which in turn has a lower viscosity than silicate melt (Tomkins et al., 2013a). Thus for a given pressure gradient in a shock vein, metal melt would be expected to accelerate and travel the most, and silicate melt to accelerate and travel the least (Tomkins et al., 2013a). This process probably contributed to the separation of metal melt from sulfide melt.

15

However, melt viscosity differences do not entirely explain why metal melt accumulated into coarser patches, or why troilite is intimately associated with silicate. To explain this, we suggest that differences in interfacial surface energies (wetting behavior) of metal and sulfide melts on solid silicate were important. Observations of meteorites (including the Portales Valley melt breccia, pallasites, IAB irons, and shock veins in chondrites) show clear textural evidence that sulfide melt distributed along the surfaces of silicates, whereas metallic melt tended to form pockets or veins more isolated from silicate (Ruzicka et al., 2005; Tomkins et al., 2013a, b; Ruzicka, 2014). This can be explained by enhanced wetting on solid silicate of sulfide melt compared to metal melt (Tomkins et al., 2013a, b). This is qualitatively consistent with experimental data which indicate lower dihedral angles for anion-rich (S-, O-rich) metallic melts than anion-poor (summarized by Rushmer et al., 2005), although experiments suggest that anion-rich melts at elevated static pressures must contain a significant amount of dissolved O to fully interconnect (Gaetani and Grove, 1999). Whether enhanced wetting of sulfide-rich melts in meteorites is a result of dynamic pressure conditions, deformation, or some other aspect of their petrogeneses is unclear. In any case, data are consistent with the idea that Fe metallic melt was non-wetting against solid silicate (e.g., Rushmer et al., 2005). This implies that once liquid metal started to accumulate within silicates, for whatever reason, it would tend to grow into a larger accumulation, thereby forming a metal nodule or a metal vein. In contrast, we speculate that sulfide melt would have more tendency to wet silicate, as shown in BM005 by troilite microveins in brecciated silicate. Coarser troilite emulsions in the BM005 veins were able to form by immiscible separation from silicate melt. But compared to metal, more troilite was distributed throughout silicate as finer grains.

Another difference between the distribution of metal and troilite in BM005 is the concentration of troilite in the inner dike, which is poor in metal. One likely critical feature is that unlike the outer dike, which was largely molten, the inner dike was partially molten. Another is that

16

the inner dike was in part physically decoupled from the outer dike in a zone of relatively low shear stress. Thus, metal-sulfide melts that in the molten outer dike were swept out of the dike in the form of shearing globules, in the inner dike instead partly became intergrown with silicates. Metal-sulfide melts that reached the troilite-rich band on the edge of the inner dike could potentially become detached from the troilite-rich band to form a globule in the outer dike. But those melts that adhered to silicate clasts in the inner dike might become trapped in the inner dike. Given different wetting tendencies for metal and sulfide melts, more of the sulfide melts and less of the metal could have been trapped in the inner dike, thereby helping to explain its troilite-rich composition.

Besides different surface energy effects that would become important after deformation ebbed, metal and sulfide melts were likely fractionated during ongoing deformation. The lack of much metal in side veins and in the dike implies that metal was more easily transported, perhaps owing to lower viscosity (Tomkins et al., 2013a). It is unlikely, for example, that surface energy effects can explain the presence in side veins of ultrafine mixes of sulfide and silicate and the absence of metal from these areas, as surface energies must be huge for such fine intermixtures and therefore less favored. Metal must be strongly depleted in such veins largely because it was preferentially transported away.

Troilite-rich veins that connect with the troilite-rich band and which are roughly perpendicular to the dike provide evidence for what we suggest is a late stage of sulfide-rich melt mobility, associated with the first stages of jointing. Veins which cross the outer dike and extend part way into the adjacent host cannot have formed while shearing was active. Instead, these veins probably represent late-stage melt that was tapped from the troilite-rich band and that was transported outward upon cooling. Troilite-rich veins that cross the inner dike probably represent melt that moved into the inner dike. Both sets of veins are roughly normal to dike and parallel to the presumed temperature gradient (cooler towards the host, and towards the center of the inner dike),

17

and were probably produced by sulfide-rich melt moving from hotter to cooler areas and filling emerging cracks.

The maximum scale of metal and sulfide mobility in BM005 can be evaluated based on estimates of the total amount of metal and sulfide in the samples studied. The inferred pre-weathered contents of troilite (<3 vol%) and metal (~2 vol%) in these samples suggest small overall depletions compared to most other L chondrites. For example, a norm of average L chondrite (Jarosewich, 1990) has 4.2 vol% troilite and 3.8 vol% metal (assuming representative mineral densities, 4.8 g/cm^3 for troilite and 7.9 g/cm^3 for metal). Similarly, utilizing published and unpublished μCT data for other L chondrites, troilite and metal contents are respectively 4.2 ± 1.4 vol% and 3.2 ± 2.3 vol% (mean and standard deviation) (Friedrich et al., 2008). Thus, the implied depletions in BM005 compared to a more typical L chondrite are roughly ≤30% for troilite and ~45% for metal. This implies that both troilite and (especially) metal were partly transported outside of the ~229 mm^3 volume of BM005 investigated with μCT. However, the amounts of inferred metal and troilite in BM005 fall within the ranges found for these chondrites, so the depletions (if real) are not overly striking. Thus, the most obvious transport effects were on a smaller scale.

Cooling conditions and parent body setting

Various features relate to the cooling history of BM005 and have implications for the parent body setting in which shock occurred. We suggest that shock melts cooled rapidly against relatively cool parent body materials, but that low-temperature annealing occurred by deep burial within the parent body.

The principal evidence for deep burial relates to the observation that metal in the host of BM005, including nodules that were likely produced by shock melting, contain grains of zoned taenite (Ni-poor cores, Ni-rich rims) coexisting with kamacite. Such metal grains are widely recognized to be the product of slow cooling under subsolidus conditions, in which kamacite grows

18

at the expense of taenite and taenite becomes increasingly Ni-rich, as required by the FeNi phase diagram and verified experimentally (e.g., Reisener and Goldstein, 2003a, b). Diffusion during cooling results in an "M-shaped" Ni profile in taenite, which for metal of L-chondrite-like composition corresponds to a formation temperature of 650-400 °C, or ~500 °C (e.g., Reisener and Goldstein, 2003a). Cooling rates can be estimated based on the central Ni content and size of zoned taenite, with the so-called central taenite method. Using a cooling formulation applicable to chondrites (Willis and Goldstein, 1981; Taylor et al., 1987; Scott et al., 2014) and the cooling rate curves of Schepker (2014), the data for BM005 fall between cooling rate curves of ~10-30 °C/Ma. Taking the fastest rate as most representative and assuming a typical precision of a factor of 2 (Scott et al., 2014), the best estimate for cooling rate in BM005 is 30 ± 30 °C/Ma at ~500 °C. Such slow cooling rates imply deep burial of BM005 at the low temperatures under which zoned taenite formed, following the shock event that created coarse metal.

In contrast, a variety of evidence suggests much faster cooling at higher temperatures, immediately after the melting event that created the dike and side veins. Rapid cooling from melt temperatures is implied by: 1) extremely sharp contacts between the host and dike, and between the host and side veins, which would not be sharp if the dike and veins remained molten for very long; 2) the magnesian band along the margins of the dike (and seen as a narrower feature also in some side veins), which is probably a chill feature produced by rapid crystallization of liquidus phases against cool host materials; 3) by the presence of shock-produced amorphous feldspar (maskelynite) close to the dike and shock veins, as opposed to feldspar, which would devitrify from glass if cooling were sufficiently slow; 4) by the presence of metal-sulfide nodules in the dike, which have cellular textures suggestive of rapid cooling; and 5) by the fine-grained textures of the dike and side veins, especially side veins composed of an ultrafine mixture of dispersed sulfide and silicate, which would not be expected to remain so finely dispersed if both were molten for very long.

19

A rough estimate of cooling rate during solidification can be obtained from models of the cooling of a molten slab, appropriate to the dike in BM005. Using the expression given by Scott (1982) based on work of Taylor and Heymann (1971), and assuming a half-width of a molten slab equal to 1.5 mm, similar to that of the dike, a cooling rate of ~280 °C/s is calculated. This implies solidification of the dike within a few seconds. Higher cooling rates are expected for the side veins, consistent with their finer grain size. If these side veins can be modeled as molten slabs with the same analytic expression, a 100-μm-wide vein would have a cooling rate of ~10^9 °C/s, implying a nearly instantaneous quench following the shock event.

An attempt was made to estimate cooling rates for metal-sulfide globules in the dike using their textures. This is based on the spacing of metal cells within troilite, using an equation given by Scott (1982) which pertains to the cooling of FeNiS metallic melts at ~950-1400 °C. Based on the data for metal cell spacings in BM005, a cooling rate of 16 x 10^3 ± 12 x 10^3 C/s (mean and standard deviation) is calculated. This cooling rate is roughly two orders of magnitude faster than implied for the cooling slab calculation, and generally faster than the cooling rates for dendritic and cellular metal-sulfide grains in other chondrites (Scott, 1982). However, we suspect the calculation for BM005 is invalid owing to the small size of dike globules (~5-40 μm and often ~15 μm in diameter), which are much smaller than the particles measured in other chondrites by Scott (1982) (~200 μm – 10 mm across). Assuming a cooling rate of ~280 °C/s as calculated from the cooling slab model, a metal cell spacing of ~13 μm would be expected, which is similar to the overall size of the globules themselves. This implies that the interior texture of the globules in BM005 cannot be used to estimate a cooling rate using the same analytic expression as for larger particles. Nonetheless, the texture of these globules resembles that of metal-sulfide particles in other chondrites that have rapid cooling rates (~1-300 °C/s; Scott, 1982).

The presence of maskelynite proximal to the dike and veins also implies rapid cooling immediately after shock melting. Feldspar glass of maskelynite-like $Ab_{80-90} An_{20-10}$ composition has a glass transition temperature of ~750 °C (740-767 °C; Arndt and Häberle, 1973), which implies that the host adjacent to the dike and side veins cooled relatively rapidly down to this temperature after shock.

Thus, it appears that BM005 cooled rapidly at higher temperatures (>950 °C and probably >750 °C) and much more slowly at lower temperatures (~500 °C). Two models to explain this can be envisioned. 1) The BM005 source region was initially cool and located at depth in the parent body, but nonetheless incorporated melt from a large impact event. In this model, pressurized melt from a strongly-heated impact site could have been rapidly injected into the BM005 chondritic protolith. Because the parent body was cool at the start, melt quenched against the chondritic wall rock. However, because the protolith was deep, and the surrounding materials were thermally insulating, heat dissipated slowly at low temperatures. Alternatively, 2) the BM005 chondritic protolith resided near the surface of the parent body, where impact melting occurred, but both protolith and melt were transported to a deeper location in the parent body as a result of impact. This could have involved catastrophic asteroidal disruption and reassembly of the sort envisioned by Taylor et al. (1987), with a fragment containing what would be BM005 becoming deeply buried during re-accretion. The initial near-surface setting involved rapid cooling because the melt was close to the cold surface of the parent body, whereas the later deep setting allowed slow cooling because heated materials were buried deeply.

We favor the first model, as there is no evidence that BM005 contained near-surface materials. However, in either model, parent body materials that were cool relative to the shock melt caused the enclosing melts to cool rapidly, and deep burial caused slow cooling at lower temperatures. To get such slow cooling at depth, the parent body at depth may have been warmed

21

close to the zoned taenite formation temperature of ~650-400 °C. Such temperatures would correspond to a low-grade thermal metamorphism.

An important role for diffusional aggregation or vapor transport?

Although we suggest that melting accompanying deformation can explain many significant aspects of the distribution of metal and sulfide in BM005, other ideas have been put forward for similar features in other chondrites. These include diffusional aggregation to form coarse metal nodules (Kong et al., 1998), vapor transport and condensation to form coarse metal nodules (Rubin, 1995, 1999; Widom et al., 1986), and vapor transport, condensation, and reaction to form intimate intergrowths of sulfide with silicate (Rubin, 2002; Rubin et al., 2001). Here we evaluate these alternatives.

It was suggested that metal nodules in two chondrites (WIS 91627 H3.7 and Jilin H5) were produced by diffusional aggregation of kamacite-rich grains along silicate grain boundaries during thermal metamorphism, based mainly on chemical data indicating the depletion of some refractory trace elements (Re, Os, Ir, Ru, Pt, Rh) in coarse metal (Kong et al. 1998). However, we do not think this interpretation is correct, for the following reasons. 1) It does not explain the relationship of nodules to shock veins and the shock dike in BM005. More generally, nodules are present in rocks that were more shocked, suggesting a shock-related origin (Rubin, 1999). 2) It does not explain the presence of coarse metal veins in BM005 and in other chondrites that also contain nodules (Widom et al., 1986; Rubin, 1999). Veins are unlikely to be produced by thermal metamorphism (Kong et al., 1998). 3) If nodules were produced by thermal metamorphism, they should be present preferentially in more metamorphosed (higher petrographic type) chondrites, but this is not true (Rubin, 1999). 4) Extensive diffusion along silicate grain boundaries over the multimillimeter- to centimeter-scale seemingly necessary for BM005 would be difficult to achieve, especially at low temperatures corresponding to the formation of zoned taenite. Extensive diffusion would be more

22

feasible at high temperatures, but would be inconsistent with evidence that BM005 cooled quickly at high temperatures.

Another possibility suggested based on data for the Faucett (H4), Slovak (H5), and Nashville (L6) chondrites is that kamacite-rich nodules formed by fractional condensation of shock-created vaporized gas in voids (Widom et al., 1986; Rubin, 1999). Although a vapor-fractionation origin could explain the trace element chemistry of some nodules that are depleted in some refractory siderophiles (Widom et al., 1986; Rubin, 1995, 1999), this model is unlikely to be the explanation for producing nodules in BM005, for the following reasons. 1) It does not explain the presence of silicates within nodules or veins in BM005. If metal condensed from gas in a void, there would be no way to suspend silicate in gas before metal could be deposited. Silicates apparently are present also within the nodules of other ordinary chondrites (Fujita et al. 1999; Kong et al., 1998), but have not been confirmed to be fully embedded in metal, as in BM005. Similarly, coarse vein metal in Portales Valley contains silicate clasts and almost certainly formed as metallic melt (Kring et al., 1999; Rubin et al., 2001; Ruzicka et al., 2005; Tomkins et al., 2013a), not as a vapor deposit. 2) Condensation does not explain the absence of voids adjacent to nodules or veins, which one would expect with the volume change accompanying the condensation of high density metal from low density vapor. 3) It is unclear why gas would concentrate in pores and not move through cracks that could easily develop in unmelted, shocked silicate. Even if vaporized gas did somehow concentrate within a given pore, it might be hot and pressurized, which could result in cracking of the surrounding silicate. However, there is no evidence for this in BM005. It should be noted that one metal vein in Densmore (1950) is associated with a crack (Widom et al, 1986), although the chemistry of this vein shows less evidence for a vapor-fractionation origin.

Therefore, we do not favor ideas that the nodules formed simply by aggregation of metal during thermal metamorphism, or by condensation. Melting was probably important in the

23

formation of nodules (Fujita et al., 1999). This can explain the composition of a nodule in the Smyer H-chondrite melt breccia, which chemically resembles that of metal + sulfide in ordinary chondrites (Rubin, 2002; D'Orazio et al., 2009). But it is certainly possible that vaporization could have affected metallic melt in some instances (Rubin, 1995), and that this process, perhaps in conjunction with crystallization processes, could explain the trace element chemistry of some nodules. The nodules in BM005 appear to be different than those present in other chondrites (Widom et al., 1986; Kong et al., 1998) in containing zoned taenite, so origins may vary between meteorites. Moreover, diffusional processes must have modified metal compositions in BM005, if zoned taenite formed by subsolidus diffusion. Similarly, there is evidence that coarse metal veins in the Kernouvé (H6) chondrite were affected by thermal metamorphism and attendant grain growth following melting and shear deformation (Friedrich et al, 2013). Therefore, thermal metamorphism as well as vaporization could have been important modifying processes in the formation of metal nodules.

Rubin (2002) suggested a vapor condensation origin for the formation of fine-scale troilite-silicate intergrowths in melt areas of the Smyer breccia. These fine-scale intergrowths resemble ultrafine mixtures of sulfide and silicate, and areas of troilite microveining, in the side veins of BM005. For Smyer, it was suggested that S vapors were liberated by the dissociation of troilite during intense shock heating, and that such vapors sulfidized fine-grained metal to once again create troilite. A similar process was envisioned to create troilite in silicate-rich areas in Portales Valley (Rubin et al., 2001). This model seems unlikely to be correct for BM005 for the following reasons. 1) If sulfide was created from a gas phase, one might expect high porosity as evidence for the former presence of gas, but some vein areas of ultrafine sulfide + silicate, and all areas of troilite-microveining, are compact and lack obvious voids. 2) There is virtually no metal in these areas in BM005, and no evidence for reaction between metal and troilite anywhere in BM005. 3) Troilite

24

microvein areas sometimes contain feldspar (or maskelynite) coexisting with sulfide in veins, which is not obviously explained by condensation. However, the presence of feldspathic microveins in the vein network is consistent with the low shock impedance of feldspar (i.e., high particle velocity for low shock pressure) over a range of shock pressures (e.g., Sharp and DeCarli, 2006), which would facilitate compression and could allow preferential melting of feldspar during shock. Both feldspar and troilite have relatively low shock impedances at pressures of ~10-20 GPa (Sharp and DeCarli, 2006). Thus, we suggest that ultrafine sulfide + silicate mixtures can be more readily explained by rapid solidification of sulfide + silicate melt, and microvein areas can be more readily explained as the result of immiscible melt containing sulfide and feldspar components wetting solid silicate.

The melt system of Buck Mountains 005

The melt system of BM005, composed of dike, side veins, and coarse metal-sulfide, is chemically variable and volumetrically small, estimated as ≤15% in the rock. The limited amount of melting probably corresponds to what was country rock below an impact crater on the parent body, where some combination of frictional melting and melt injection occurred during a moderately strong shock event. Within the melt system, there were spatial variations in original deformation extent, melting degree, and ultimate composition, all on a small scale (<1 cm^3). Some areas were highly sheared, largely melted, and silicate-rich (the outer dike); some areas were highly-sheared, largely melted, and rich in FeNi metal (metal-rich nodules and metal-rich veins); and still other areas were substantially melted, metal-poor, and locally variable in composition and deformation extent (the inner dike and side veins).

IMPLICATIONS

Our results provide support for the idea that metallic melts can be mobilized by shear deformation (Bruhn et al., 2000; Groebner and Kohlstedt, 2006; Kohlstedt and Holzman, 2009; Rushmer et al., 2000, 2005; Rushmer and Petford, 2011) and that melting and shear conditions

25

necessary for mobilization can occur as a result of collisional processes (e.g., Ruzicka et al., 2005; Tomkins et al., 2013a). They support the idea that shock melting and deformation can result in the segregation of metal from sulfide (e.g., Tomkins et al., 2013a).

Given the low degree of overall melting and small spatial scale of fractionations in BM005, the question arises as to whether similar melting and fractionation effects could have been important on a larger scale in planetesimals, and whether this could have resulted in core formation. Based on data for other meteorites, we suggest that similar melting and segregation processes frequently occurred on a larger scale, and that core formation could have been triggered under some circumstances.

There is good evidence for the occurrence of similar but larger scale processes. Metal nodules, often larger than those found in BM005, are relatively common features in ordinary chondrites (Rubin, 1999). Impact melting has been inferred for small metal-rich meteorites of ordinary chondrite affinity, including meteorites classified as "H metal" (Sacramento Wash 005, 52.3 g total known weight; LEW 88432, 1.3 g) and "ungrouped iron" (MET 00428, 45.8 g; Sahara 03505, 65 g) (D'Orazio et al., 2009; Schrader et al., 2010). Metal compositions in these meteorites are similar to those in ordinary chondrites, and to a nodule in Smyer, suggesting a similar origin by impact melting of ordinary chondrite (D'Orazio et al., 2009; Schrader et al., 2010). The comparatively large masses of the recovered metal-rich specimens indicate melting on a bigger scale than in BM005.

One of the small metal-rich meteorites, Sacramento Wash 005 (Schrader et al., 2010), contains adhering H chondrite and was found in the same dense collection area (DCA), now known as the Yucca DCA, as Buck Mountains 005 (MBD, 2014). The Yucca DCA contains hundreds of recovered specimens from at least six different ordinary chondrite falls, including many small irons of mass ~1-2 g that were probably liberated from one or more of the chondrites as nodules during

26

meteor ablation (Hutson et al., 2013a). One of the chondrites (Buck Mountains Wash, H3-6) in the Yucca DCA contains nodules as well as silicate-rich melt areas, and a different unpaired chondrite (Franconia, H5) contains a prominent metallic vein (Hutson et al., 2013a). Thus, the Yucca meteorites apparently show evidence for the frequent production of metallic impact melts.

The situation for BM005, involving limited amounts of silicate melting overall but the presence of coarse metal that was molten, could be analogous to the situation for some silicate-bearing iron meteorites, especially the IAB/IIICD irons, and the unfractionated IIE irons (see review by Ruzicka, 2014). One suggested origin for such irons is impact melting with preferential melting of metal and sulfide, and much less melting of silicates (Ruzicka, 2014, and references therein). The evidence from partly shock melted chondrites such as BM005, as well as studies of IAB irons such as Campo del Cielo, seems to support the idea that impact processes were important in the formation of such irons, whereby the irons could correspond to larger accumulations of metal-rich pods produced by impact segregation (Tomkins et al., 2013a). Continued heating of bodies containing large metal-rich pods could even ultimately result in core formation (Tomkins et al., 2013a, b). Such heating could potentially arise from repeated impacts, or by internal heating via decay of short-lived radionuclides such as ^{26}Al.

However, the data also suggest a difference between BM005 and the irons. In BM005, melting of metal and sulfide was accompanied by melting of silicate as well, although it is true that the system overall was little-melted. In the irons, in contrast, a much larger amount of coarse metal was clearly molten, but a smaller amount of silicate was melted. This suggests that IAB-related irons and unfractionated IIE irons containing chiefly coarse metal and unmelted silicate did not form in a completely analogous manner to BM005. Although it seems that impact processes can result in somewhat large metal accumulations, it is not clear that larger irons can be formed this way.

27

One variable that could explain the differences between irons and BM005 is the thermal state of the parent asteroidal bodies at the time of impact. If the asteroids were hot, it might be possible to mobilize metal more efficiently, either during or after deformation, even if silicate were largely unmelted. This type of model, invoking both collisions and an endogenic process such as decay of ^{26}Al to heat asteroid interiors, can potentially explain a wide variety of silicate-bearing iron meteorites and stony-iron meteorites (Ruzicka, 2014; and references therein), as well as chondrites such as Portales Valley (Ruzicka et al., 2005) and Kernouvé (Friedrich et al., 2013) (also Ruzicka, Hugo and Hutson, 2015, submitted to GCA). With an already warm target, impact-triggered core formation is an attractive possibility.

ACKNOWLEDGMENTS

REFERENCES CITED

Arndt, J, and Häberle, F. (1973) Thermal expansion and glass transition temperatures of synthetic glasses of plagioclase-like compositions. Contributions to Mineralogy and Petrology, 39, 175-183.

Brown, R., Ruzicka, A., Friedrich, J., Hutson, M., and Rivers M. (2013a) A shock melt dike in 3D: Shear and melt migration in the Buck Mountains 005 L6 chondrite. Meteoritics & Planetary Science, 76, Supplement, Abstract #5078.

28

Brown, R., Ruzicka, A.M., Hutson, M., Friedrich, J.M., and Rivers, M.L. (2013b) Micro-tomography and electron microscopy of a shock dike in the Buck Mountains 005 L6 chondrite. In AGU Fall Meeting Abstracts, Vol. 1, p. 1808.

Bruhn, D., Groebner, N., and Kohlstedt, D.L. (2000) An interconnected network of core-forming melts produced by shear deformation. Nature, 403, 883-886.

D'Orazio, M., Folco, L., Chaussidon, M., and Rochette, P. (2009) Sahara 03505 sulfide-rich iron meteorite: Evidence for efficient segregation of sulfide-rich metallic melt during high-degree impact melting of an ordinary chondrite. Meteoritics & Planetary Science, 44, 221–231.

Ebel, D.S. and Rivers, M.L. (2007) Meteorite 3-dimensional synchrotron microtomography: methods and applications. Meteoritics & Planetary Science, 42, 1627–1646.

Friedrich, J.M., Wignarajah, D.P., Chaudhary, S., Rivers, M.L., Nehru, C.E., and Ebel, D.S. (2008) Three-dimensional petrography of metal phases in equilibrated L chondrites—Effects of shock loading and dynamic compaction. Earth and Planetary Science Letters, 275, 172–180.

Friedrich, J.M., Ruzicka, A., Rivers, M.L., Ebel, D.S., Thostenson, J.O., and Rudolph, R.A. (2013) Metal veins in the Kernouvé (H6 S1) chondrite: Evidence for pre- or syn-metamorphic shear deformation. Geochimica et Cosmochimica Acta, 116, 71–83.

Fujita, T., Kojima, H., and Yanai, K. (1999) Origin of metal-troilite aggregates in six ordinary chondrites. Antarctic Meteorite Research, 12, 19-35.

Gaetani, G.A., and Grove, T.L. (1999) Wetting of mantle olivine by sulfide melt: implications for Re/Os ratios in mantle peridotite and late-stage core formation. Earth and Planetary Science Letters, 169, 147-163.

29

Groebner, N., and Kohlstedt, D.L. (2006) Deformation-induced metal melt networks in silicates: Implications for core–mantle interactions in planetary bodies. Earth and Planetary Science Letters, 245, 571–580.

Hörz, F., Cintala, M.J., See, T.H., and Loan, L. (2005) Shock melting of ordinary chondrite powders and implications for asteroidal regoliths. Meteoritics & Planetary Science, 40, 1329–1346.

Huss, G.R., Rubin, A.E., and Grossman, J.N. (2005) Thermal metamorphism in chondrites. In D.S. Lauretta and H.Y. McSween Jr., Eds., Meteorites and the Early Solar System, p. 567-586. The University of Arizona Press, Tucson.

Hutson, M., Ruzicka, A., Jull, T., Smaller, J., and Brown, R. (2013a) Stones from Mohave County, Arizona: Multiple falls in the "Franconia strewn field". Meteoritics & Planetary Science, 48, 365-389.

Hutson, M., Ruzicka, A., and Brown, R. (2013b) A pyroxene-enriched shock melt dike in the Buck Mountains 005 (L6) chondrite. 44th Lunar and Planetary Science Conference, Abstract #1186.

Jamsja, N. and Ruzicka, A. (2010) Shock and thermal history of NWA 4859, an annealed impact-melt breccia of LL-chondrite parentage containing unusual igneous features and pentlandite. Meteoritics & Planetary Science, 45, 828-849.

Jarosewich, E. (1990) Chemical analyses of meteorites: A compilation of stony and iron meteorite analyses. Meteoritics, 25, 323–337.

Ketchum, R.A. (2005) Computational methods for quantitative analysis of three dimensional features in geological specimens. Geosphere, 1, 32–41.

Kohlstedt, D.L., and Holtzman, B.K. (2009) Shearing melt out of the Earth: An experimentalist's
perspective on the influence of deformation on melt extraction. Annual Review of Earth and
Planetary Sciences, 37, 561-593.

Kong, P., Ebihara, M., and Xie, X. (1998) Reevaluation of formation of metal nodules in ordinary
chondrites. Meteoritics & Planetary Science, 33, 993-998.

Kring, D.A., Hill, D.H., Gleason, J.D., Britt, D.T., Consolmagno, G.J., Farmer, M., Wilson, S., and
Haag, R. (1999) Portales Valley: A meteoritic sample of the brecciated and metal-veined
floor of an impact crater on an H chondrite asteroid. Meteoritics & Planetary Science, 34,
663–669.

MBD (2014) Meteoritical Bulletin Database. http://www.lpi.usra.edu/meteor/metbull.php. Accessed
October 6, 2014.

Minarik, W.G., Ryerson, F.J., and Watson, E.B. (1996) Textural entrapment of core-forming melts.
Science, 272, 530-533.

Passchier, C.W., and Trouw, R.A.J. (2005) Microtectonics, 366 p. Springer-Verlag, Heidelberg.

Reisener, R.J., and Goldstein, J.I. (2003a) Ordinary chondrite metallography: Part 1. FeNi taenite
cooling experiments. Meteoritics & Planetary Science, 38, 1669-1678.

Reisener, R.J., and Goldstein, J.I. (2003b) Ordinary chondrite metallography: Part 2. Formation of
zoned and unzoned metal particles in relatively unshocked H, L, and LL chondrites.
Meteoritics & Planetary Science, 38, 1679-1696.

Rubin, A.E. (1995). Fractionation of refractory siderophile elements in metal from the Rose City
meteorite. Meteoritics, 30, 412-417.

Rubin, A.E. (1999) Formation of large metal nodules in ordinary chondrites. Journal of Geophysical
Research 104, 30799–30804.

31

Rubin, A.E. (2002) Smyer H-chondrite impact-melt breccia and evidence for sulfur vaporization. Geochimica et Cosmochimica Acta, 66, 699–711.

Rubin, A.E., Ulff-Møller, F., Wasson, J.T., and Carlson, W.D. (2001) The Portales Valley meteorite breccia: Evidence for impact induced melting and metamorphism of an ordinary chondrite. Geochimica et Cosmochimica Acta, 66, 323–342.

Rushmer, T., and Petford, N. (2011) Microsegregation rates of liquid Fe-Ni-S metal in natural silicate-metal systems: A combined experimental and numerical study, Geochemistry Geophysics Geosystems, 12, Q03014, doi:10.1029/2010GC003413.

Rushmer, T., Minarik, W.G., and Taylor, G.J. (2000) Physical processes of core formation. In R.M. Canup and K. Righter, Eds., Origin of the Earth and Moon, p. 227-243. The University of Arizona Press, Tucson.

Rushmer, T., Petford, N., Humayun, M., and Campbell, A.J. (2005) Fe-liquid segregation in deforming planetesimals: Coupling core-forming compositions with transport phenomena. Earth and Planetary Science Letters 239, 185–202.

Ruzicka, A. (2014) Silicate-bearing iron meteorites and their implications for the evolution of asteroidal parent bodies. Chemie der Erde, 74, 3–48.

Ruzicka, A., Killgore, M., Mittlefehldt, D.W., and Fries, M. (2005) Portales Valley: Petrology of a metallic-melt meteorite breccia. Meteoritics & Planetary Science, 40, 261-295.

Ruzicka, A., Grossman, J. N., and Garvie, L. (2014) The Meteoritical Bulletin, No. 100, 2014 June. Meteoritics & Planetary Science, 49, E1-E101, August 2014.

Schepker, K.L. (2014) Complex thermal histories of L melt breccias NWA 5964 and NWA 6580, 94 p. MS Thesis, Portland State University, Paper 1835.

Schmitt, R.T. (2000) Shock experiments with the H6 chondrite Kernouvé: Pressure calibration of microscopic shock effects. Meteoritics & Planetary Science, 35, 545-560.

32

Schrader, D.L., Lauretta, D.S., Connolly, H.C., Goreva, Y.S., Hill, D.H., Domanik, K.J., Berger, E. L., Yang, H., and Downs, R.T. (2010) Sulfide-rich metallic impact melts from chondritic parent bodies. Meteoritics & Planetary Science, 45, 743–758.

Scott, E.R.D. (1982) Origin of rapidly solidified metal-troilite grains in chondrites and iron meteorites. Geochimica et Cosmochimica Acta, 46, 813-823.

Scott, E.R.D., Krot, T.V., Goldstein, J.I., and Wakita, S. (2014) Thermal and impact history of the H chondrite parent asteroid during metamorphism: Constraints from metallic Fe-Ni. Geochimica et Cosmochimica Acta, 136, 13-37.

Sharp, T.G. and DeCarli, P.S. (2006) Shock effects in meteorites. In D.S. Lauretta and H.Y. McSween Jr., Eds., Meteorites in the Early Solar System II, p. 653-677. The University of Arizona Press, Tucson.

Shannon, M.C., and Agee, C.B. (1996) High pressure constraints on percolative core formation. Geophysical Research Letters, 23, 2717-2720.

Spray, J.G. (2010) Frictional melting processes in planetary materials: From hypervelocity impact to earthquakes. Annual Review of Earth and Planetary Sciences, 38, 221–254.

Stöffler, D., Keil, K., and Scott E.R.D. (1991) Shock metamorphism of ordinary chondrites. Geochimica et Cosmochimica Acta, 55, 4845-3867.

Taylor, G.I. and Heymann, D. (1971) Postshock thermal histories of reheated chondrites. Journal of Geophysical Research, 76, 1879-1893.

Taylor, G.J., Maggiore, P., Scott, E.R., Rubin, A.E., and Keil, K. (1987) Original structures, and fragmentation and reassembly histories of asteroids: Evidence from meteorites. Icarus, 69, 1-13.

Tomkins, A.G., Weinberg, R.F., Shaefer, B.F., and Langendam, A. (2013a) Disequilibrium melting

and melt migration driven by impacts: Implications for rapid planetesimal core formation.

Geochimica et Cosmochimica Acta, 100, 41–59.

Tomkins, A.G., Mare, E.R., and Raveggi, M. (2013b) Fe-carbide and Fe-sulfide liquid immiscibility

in IAB meteorite, Campo del Cielo: Implications for iron meteorite chemistry and

planetesimal core compositions. Geochimica et Cosmochimica Acta, 117, 80–98.

van der Bogert, C.H., Schultz, P.H., and Spray, J.G. (2003) Impact-induced frictional melting in

ordinary chondrites: A mechanism for deformation, darkening, and vein formation.

Meteoritics & Planetary Science 38, 1521-1531.

Widom, E., Rubin, A.E., and Wasson, J.T. (1986) Composition and formation of metal nodules and

veins in ordinary chondrites. Geochimica et Cosmochimica Acta, 50, 1989–1995.

Willis, J. and Goldstein, J.I. (1981) A revision of metallographic cooling rate curves for chondrites.

Proceedings of the Lunar and Planetary Science Conference, 13B, 1135-1143.

Figure captions.

Figure 1. (a) Image of complete hand specimen of Buck Mountains 005 (sample 0491-5)

used for microtomography studies prior to serial sectioning. The dike cross-cuts the entire

specimen, and has a columnar surface expression on broken (non fusion-crusted) surfaces as seen

here, with columns perpendicular to the dike. One of two localized dark surface patinas is visible at

lower right. **(b)** Image of cut face of 0491-5, obtained by making a cut roughly perpendicular to the

dike on the right side of the specimen shown in part a. The dike appears as a dark feature, as do

thinner branching and subparallel side veins. Coarse metal is present at the edge of the specimen at

left and upper right, where it forms sheets along the sample edge. **(c)** Closer view of metal exposed

34

at the edge of the specimen immediately below the patina in part a. The patina occurs on a slightly

raised but generally flat surface (a metal-rich sheet).

Figure 2. Images of the shock dike in polished thin sections. **(a)** Transmitted light binocular

image of section 0491-3A, showing the shock dike with inner-outer dike zonal structure (clasts

more prevalent in the inner dike), subparallel side veins, and a larger branching side vein. Box d

shows a region magnified in part d. **(b)** Backscattered electron (BSE) image mosaic of section

0491-5-2, showing a depletion of larger metal and sulfide grains (bright grains) within the dike, the

presence of coarse metal within the meteorite host, and cracks cutting across the dike at a high

angle. Weathering product (w.p., bright) forms a sheet-like structure at the left edge of the section

and partly fills the high angle cracks. Box c shows a region magnified in part c. **(c)** BSE image of

0491-5-2 showing the fine-grain size of the dike compared to the host, a troilite-rich band at the

edge of the inner dike, a depletion of troilite in the outer dike except for some globules (one larger

globule near the troilite-rich band and many smaller ones near the contact with the host), a troilite-

rich vein (v), and the presence of clasts in the inner dike. ol = olivine, opx = orthopyroxene. **(d)**

BSE image of 0491-3A showing the intersection of the dike with the prominent side vein in part a,

including the presence of many troilite-rich globules in both the outermost portion of the dike and in

the side vein, and a magnesian band (darker grey) in the outer dike composed of mafic silicates that

bulge into the side vein. Symbols same as in part c, and also phos = phosphate, feld = feldspar /

maskelynite. **(e)** BSE image of 0491-3A showing the presence of mafic dike silicates (olivine,

pyroxene), some apparent clasts and some with euhedral outlines, within the troilite-rich band at the

margin of the outer dike. The band is composed of both troilite (brighter) and weathering product of

metal (w.p.). **(f)** BSE image of the outer dike in 0491-3A, showing three globules composed of

various amounts of metal (nearly-white), troilite (light grey), and weathering product of metal

35

(w.p.). In metal-troilite globules, metal forms cells within troilite. Fe-(hydr)oxide symplectite is interstitial to mafic silicates.

Figure 3. Images of side veins and associated coarse metal in section 0491-5-2. **(a)** Plane-polarized transmitted light image mosaic showing a network of dark-appearing branching and subparallel side veins adjacent to the dike. Boxes b, c, and d show areas magnified in parts b, c, and d. **(b)** Reflected light image mosaic of the coarse metal (nearly white) showing entry points of silicate-rich veins (1, 2, 3, 4, 5). Coarse metal is composed of kamacite (kam), taenite (tae), and plessite (pl), and is associated with a smaller amount of coarse troilite (troi). Weathering product (w.p.) is concentrated at the edge of the section adjacent coarse metal. **(c)** BSE image showing the intersection of a silicate-rich side vein with coarse metal (location 2 in part b). Symbols same as in Fig. 2b and 3b. **(d)** BSE image mosaic of a fine-grained, clast-laden branching side vein that shows variations in the texture and proportion of troilite (bright). Parts of the vein are troilite-poor and enriched in silicate (S), but other areas are enriched in ultrafine troilite (T) or enriched in troilite-rich globules (G). The largest clast is flanked by a troilite emulsion (E) at one edge, and internally is brecciated with interstitial veins composed of troilite (troi), troilite + feldspar (troi + feld), or feldspar. Symbols same as in Fig. 2c and also cpx = Ca-pyroxene.

Figure 4. Micro-CT tomogram image slices of sample 0491-5 showing metal (white), troilite and weathering product (light grey), silicate (medium grey), and void (black). These slices have a perspective similar to Fig. 1b and 2b, rotated ~90 ° counterclockwise, and were obtained at successive depths in the sample (numbers at upper right indicate relative distance in microns from the first tomogram in part a). Brackets indicate the location of the dike. **(a)** Both the outer dike (OD) and inner dike (ID) are visible, the latter by a brighter appearance at the margins (troilite-rich bands). The ID has thicker and thinner areas. Several microcracks partly filled with weathering product (or troilite) are enclosed within and roughly perpendicular to the dike. A silicate clast is

36

visible in the ID. **(b)** The ID is comprised of two boudin-like structures (1, 2); asymmetry in boudin 1 is consistent with dextral shear on opposite sides of the ID (arrows). **(c)** A coarse nodule composed of metal and sulfide / weathering product and enclosing silicate is present in the host next to the dike. The adjacent OD contains globules. The dike is entirely OD material except for a single boudin-like feature (1) that represents the ID. **(d)** Three coarse nodules composed largely of metal are visible in the host, including the one from part c. The ID is composed of two asymmetric boudin-like structures consistent with dextral shear.

Figure 5. 3D models showing the distribution of metal (white) and troilite / weathering product (grey) in sample 0491-5 based on micro-CT data. The perspective is similar to that in Fig. 4. **(a)** Metal distribution. The dike is almost metal-free, whereas the host contains large metal nodules at different distances from the dike. The largest eight nodules are numbered according to decreasing volume; nodules 1 (~0.86 mm^3), 8 and 4 are visible in Fig. 4d; nodule 2 (~0.45 mm^3), which may be an extension of the coarse metal studied in thin section (Fig. 3b) and in saw cuts (Fig. 1b, upper right surface) is visible in Fig. 4a. (b) Troilite and weathering product distribution. Both are depleted in the outer dike (OD), but are concentrated in the inner dike (ID) in sheet-like structures parallel to the dike long axis (probably mainly troilite-rich bands). The OD contains sheet-like structures perpendicular to the dike (probably both weathering product and troilite-rich veins).
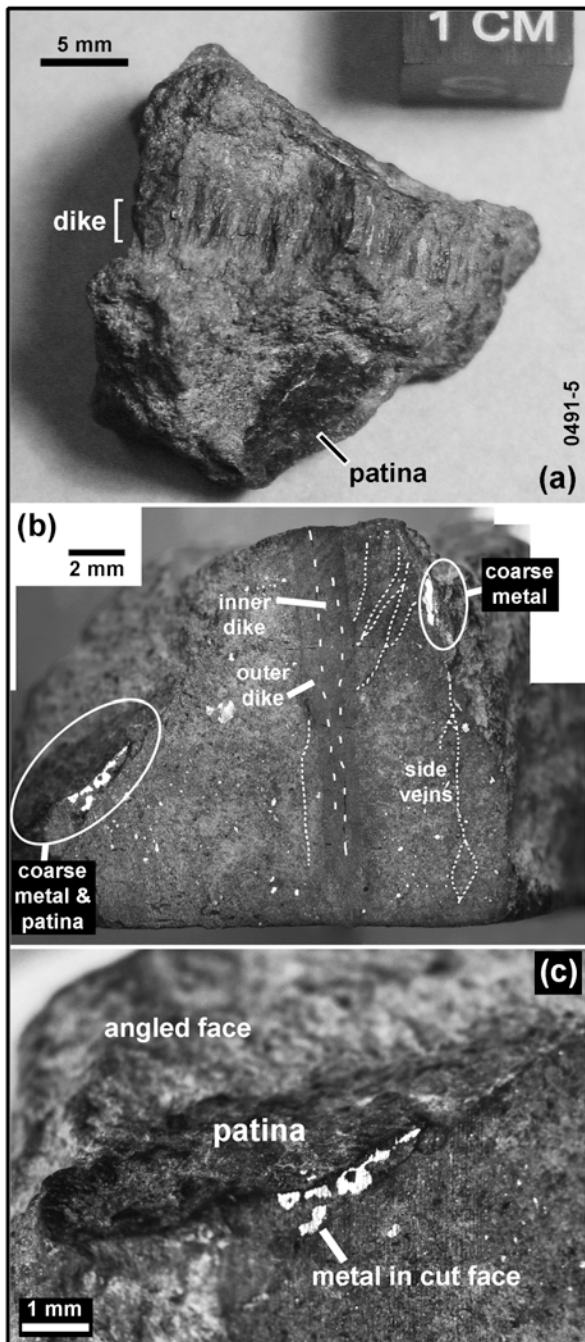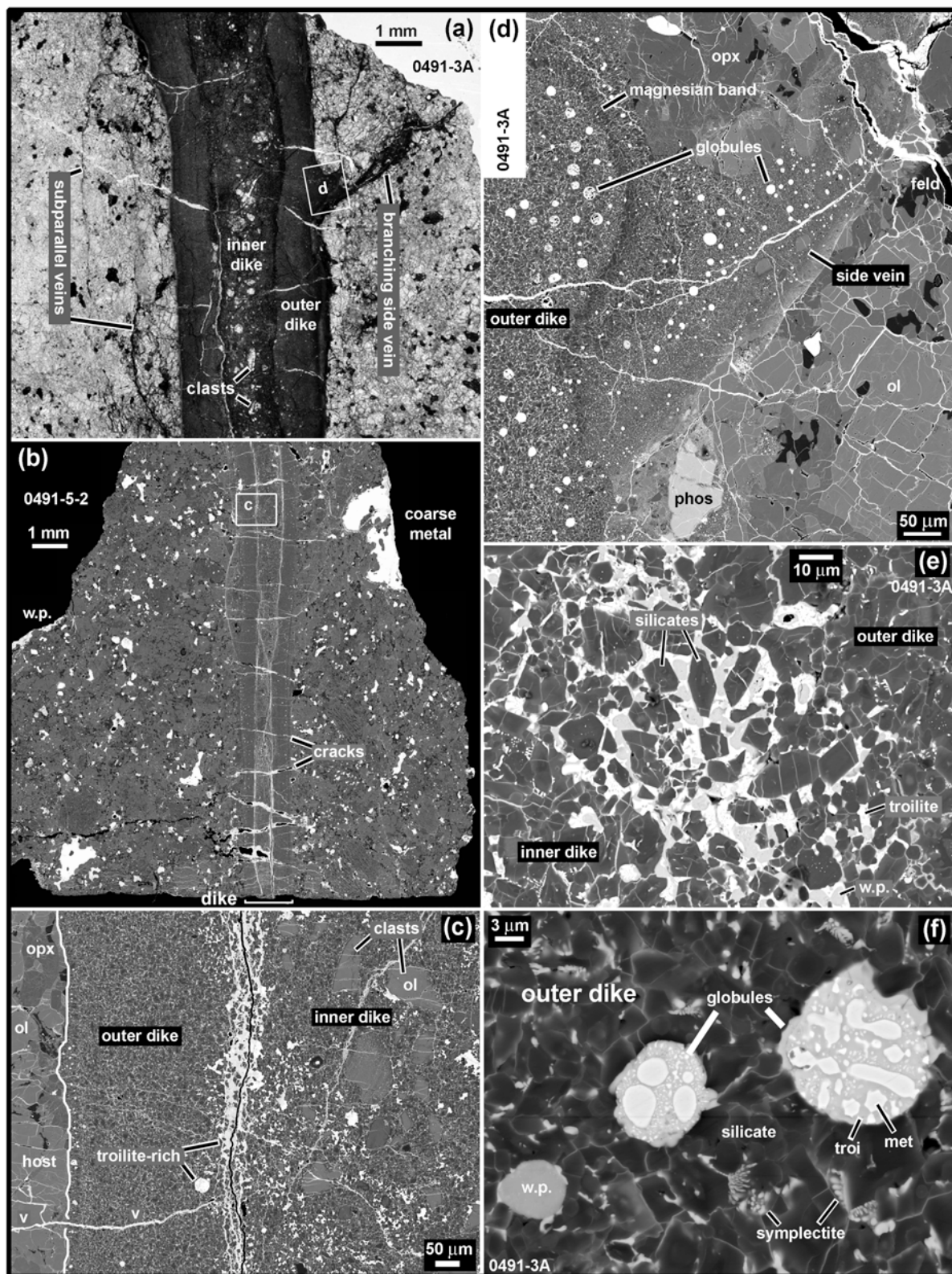
37

Figure 1
(3.18" w x 7.15" h, 475 dpi)

38

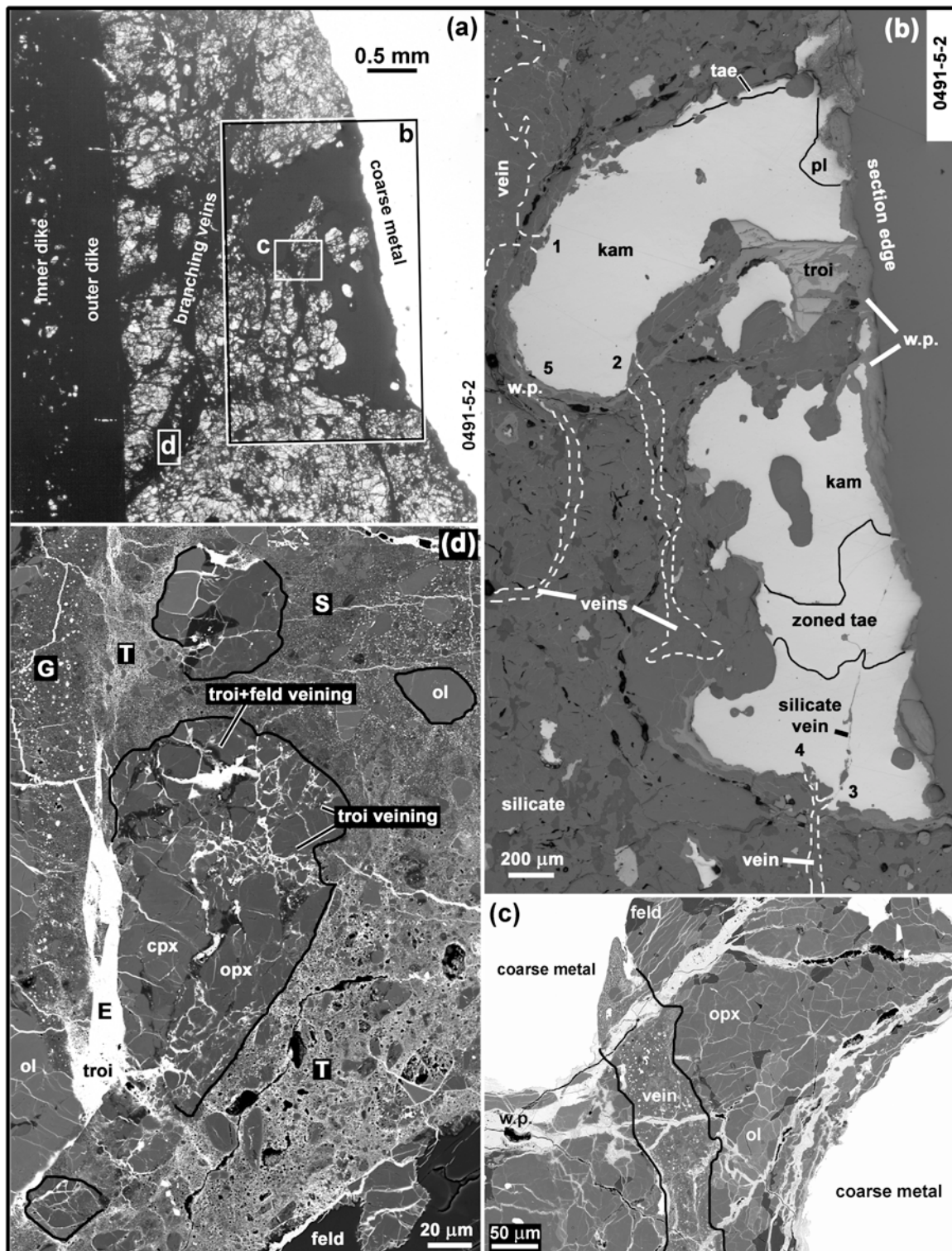Figure 2
(6.65" w x 8.57" h, 450 dpi)

39

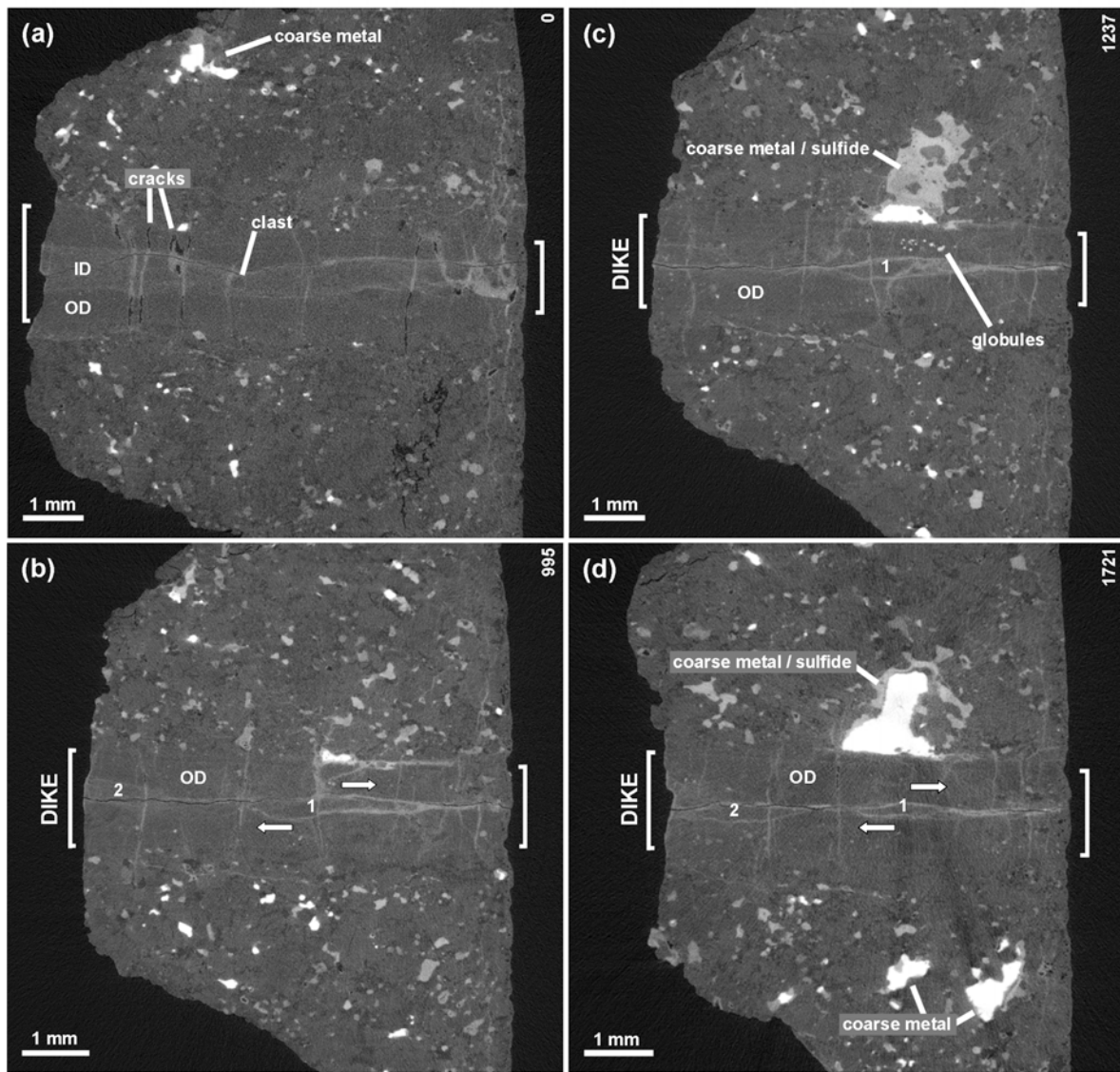Figure 3
(6.15" w x 7.95" h, 600 dpi)

40

Figure 4
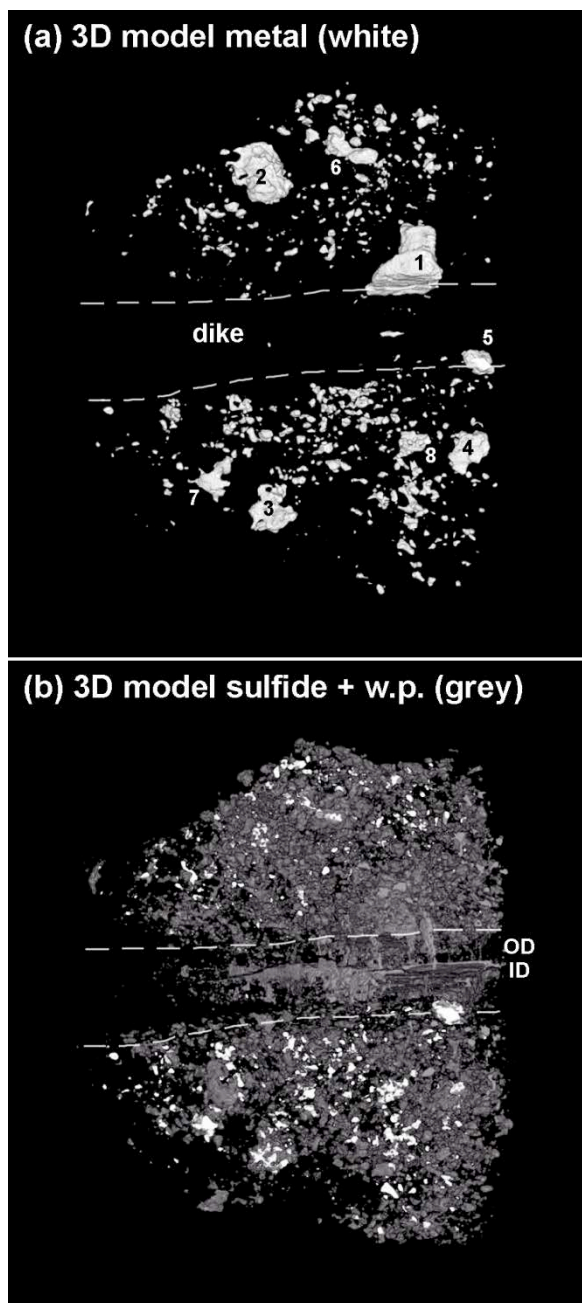(7.17" w x 6.84" h, 310 dpi)

41

Figure 5
(3.0" w x 6.78" h, 300 dpi)

Table 1. Modal data for Buck Mountains 005 based on reflected light (RL), chemical (EDS), and micro-CT mapping

	0491-3A section	0491-5-2 section		0491-5-2 section	0491-5-2 host [a]	0491-5-2 inner dike	0491-5-2 outer dike	0491-5-2 dike [b]		0491-5 piece
Technique	RL	RL		EDS	EDS	EDS	EDS	EDS		Micro-CT
Resolution (µm/pixel)	4.3	4.1		4.1	4.1	4.1	4.1	4.1	Resolution (µm/voxel)	7.72, 9.32
Area (mm²)	239.2	203.9		269.4	236.0	13.1	20.4	33.5	Volume (mm³)	228.7
Area (%)			**Area (%)**						**Vol. (%)**	
Metal	0.9 (<0.1)	2.0 (<0.1)	Metal	2.5 (0.2)	4.0 (0.1)	Trace	Trace	Trace	Metal	0.97
Troilite	1.0 (0.1)	1.0 (<0.1)	Troilite	1.5 (<0.1)	1.6 (0.1)	3.3 (0.2)	1.4 (0.4)	2.1 (0.3)	Troilite + hydroxide	4.71
Oxide + hydroxide	7.6 (0.4)	4.3 (<0.1)	Hydroxide	7.1 (1.1)	7.2 (0.3)	16.0 (1.0)	6.4 (0.5)	9.8 (0.7)	Other	94.32
Silicate	90.5 (0.5)	92.8 (0.1)	Mafics [c]	73.9 (2.9)	71.8 (2.0)	77.8 (1.4)	90.6 (0.1)	86.0 (0.6)		
			Ca-pyroxene	3.2 (0.2)	3.1 (0.6)	0.24 (0.02)	n.d.	0.1 (0.01)		
			Feldspar	8.8 (0.8)	11.1 (0.5)	2.5 (0.8)	1.3 (0.1)	1.7 (0.3)		
			Phosphate	1.4 (0.1)	0.4 (<0.1)	n.d.	n.d.	n.d.		
			Chromite	0.6 (<0.1)	0.8 (0.1)	0.26 (0.02)	0.2 (0.2)	0.2 (0.1)		

Note: Values in parentheses give uncertainties (precision). n.d. = not detected. Hydroxide is terrestrial weathering product.
[a] Includes everything that is not dike. [b] Calculated from inner and outer dike data. [c] Mafic silicates, includes olivine, low-Ca pyroxene, and various pyroxene-like phases in dike.